ACS APPLIED MATERIALS & INTERFACES

Research Article

www.acsami.org

Controlled Seeding of Laser Deposited Ta:TiO_2 Nanobrushes and Their Performance as Photoanode for Dye Sensitized Solar Cells

Yukihiro Hara,*[,†] Timothy Garvey,[†] Leila Alibabaei,[‡] Rudresh Ghosh,[†,§] and Rene Lopez[†]

[†]Department of Physics and Astronomy and [‡]Department of Chemistry, University of North Carolina at Chapel Hill, Chapel Hill, North Carolina 27599, United States

ABSTRACT: Hexagonal patterned indium tin oxide (ITO) with a height of 1.5 μm was fabricated on fluorinated SnO_2 (FTO) substrate via nanoimprint lithography and pulsed laser deposition (PLD). Tantalum doped TiO_2 was deposited on the patterned substrate by PLD. The film of Ta:TiO_2 grew vertically and separately on the patterned ITO and formed a brush-like structure. Dye-sensitized solar cells with the Ta:TiO_2 film deposited on the patterned substrate as well as flat FTO substrate for comparison were fabricated and tested. The device with the patterned substrate showed a 25% increase in short circuit current (J_{sc}) compared to the one with flat FTO substrate. Optical and photoelectrochemical characterization techniques were performed to investigate the improvement. The increase of J_{sc} was attributed to the enhancements of light absorption in the 600−750 nm range and collection of excited electrons by the brush-like structure and the patterned ITO, respectively.

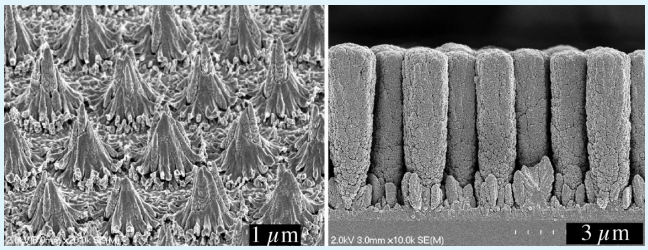

KEYWORDS: *dye sensitized solar cells, pulsed laser deposition, tantalum doped titanium oxide, nanoimprint lithography, hierarchical structure, photoelectrochemistry*

INTRODUCTION

Invented by Grätzel et al.[1] in 1991, dye sensitized solar cells (DSSCs) have received much attention as an alternative photovoltaic technology because of its relatively low intrinsic materials cost and their ease of fabrication. DSSCs differ from conventional semiconductor devices in that they separate the function of light absorption from charge carrier transport. Typical DSSCs[2−4] combine a solid, wide-bandgap semiconductor with a liquid ionic conductor containing a redox couple, typically I_3^-/I^-. The photoanode is made of a layer of a few micrometers of titanium dioxide nanocrystals on which a dye, usually a ruthenium polypyridyl complex, is adsorbed. This nanocrystalline film is built on a transparent conductive substrate, typically indium tin oxide (ITO) or fluorinated SnO_2 (FTO), and sandwiched with a redox I_3^-/I^- electrolyte and a platinum coated conductive substrate. Diffusion driven and free of electric fields,[5−7] an important source of losses is the quality of the electron transport in the nanoparticle network. The film needs to be ∼10 μm thick to accommodate enough dye molecules, a metric barely commensurable with electron diffusion length (< 10 μm).[8,9] The fact that the light absorption and transport lengths are similar has allowed DSSCs to reach notable efficiencies. With champion cell efficiencies above 12%, DSSCs have already been used in commercial niche-level applications.

To realize the full potential of the DSSC concept, numerous dyes, electrolytes, semiconducting materials, and nanostructures have been extensively investigated to improve the DSSC's photoconversion efficiency. In particular regarding transport, researchers have focused their efforts in modifying the oxide semiconductor transport properties with nanostructures and compositions that maximize diffusion lengths of excited electrons. TiO_2 and other oxide semiconductor nanorods or nanotubes[10−14] have been tried as replacements for nanoparticles, in particular aligned rods seemed to provide an intuitive venue to improve electron diffusion. Unfortunately, such novel nanostructures have not been very successful. The main reason for this is that crystalline oxide nanorods simply do not provide enough surface area in thin film of reasonable thickness.[15] In 2011 Grätzel[16] introduced a novel photoanode with a nanoscale structure that resembled a forest, fabricated by pulsed laser deposition (PLD) under relatively high background gas pressures. This new nanostructure, which they named "nanoforest", replaces the traditional random nanoparticle oxide network by vertically aligned bundles of TiO_2 oxide nanocrystals. Combining the high surface area of nanoparticles with the electron transport directionality of vertical rods has proven effective by several groups,[16−18] and more recently, we have demonstrated further transport improvements by tantalum doping of the TiO_2 nanoforest.[19]

It is also relevant to point out that in contrast with the numerous efforts to nanostructure the oxide semiconductor, there have been relatively few studies concerning the modification of the conductive substrate to improve the performance. Besides high transparency and suitable sheet resistance, this essential part of the device is usually not

Received: September 24, 2013
Accepted: December 9, 2013
Published: December 9, 2013

required to perform additional roles. However, one can consider structurally modifying the conductive substrate as a means to enhance light trapping and/or improve collection of charge carriers. In regards to the first possibility for example, in 2012 Wang et al.[20] patterned FTO substrates via reactive ion etching (RIE) which were incorporated as the anode in DSSCs. These DSSCs showed improved efficiencies compared to DSSCs fabricated using unpatterned FTO anodes, and the enhancement was attributed to increased light scattering by the patterned FTO anode. Furthermore, as DSSCs are dominated by diffusion and kinetic factors, to improve the collection of electrons, patterning of the transparent conductor could be used to lessen the demands of transport length.

In this paper, we demonstrate a 25% improvement in short circuit current (J_{sc}) achieved by building a photoanode that realizes the best of the ideas discussed above, namely, an ordered patterned microstructure of the transparent conductor substrate is introduced which combined with the PLD nanoforest Ta:TiO_2 growth, results in a highly ordered and hierarchical structure at all the relevant length scales. Very interestingly, and likely a key feature behind the current enhancement, the spike-like morphology of the patterned ITO functions as "nucleation" sites that govern the growth of individual Ta:TiO_2 nanobrushes. The growth process prevents the deposition of Ta:TiO_2 onto areas between brushes resulting in separated Ta:TiO_2 brushes each of which possess a trunk of highly conductive oxide and exhibit large surface area foliage. Large area microfabrication of these arrays is achieved by utilizing soft nanoimprint lithography masters and standard high throughput nanofabrication techniques.

EXPERIMENTAL SECTION

Fabrication of Hexagonally Arranged ITO Spikes on FTO Substrates. The fabrication process (Figure 1) for the patterned conductive substrate starts by first forming a 2-D hexagonal pattern of circular holes in a SU-8 layer with chromium mask raised from the FTO substrate. Next, pulsed laser deposition (PLD) was used to fill these holes with ITO, and then the mask and SU-8 were subsequently removed. FTO glasses (Hartford Glass) were cleaned by ultrasound for 15 min in baths of deionized H_2O, isopropanol, and acetone in sequence. The FTO substrates were then subjected to O_2 plasma prior to the deposition of photoresists by spin coating. SU-8 2000.5 (Microchem) was cast at a spinning rate of 1000 rpm applied for 40 s, and the resulting films were exposed to UV, then cured for 2 min at 60 °C followed by 2 min at 95 °C. The thickness of this layer is important because the height of the final ITO spikes depends on the depth of the holes. A mixture of 495 PMMA and 950 PMMA (Microchem) (1:1 = v:v) was cast at a spinning rate of 3000 rpm applied for 40 s, and the films were heated at 180°C for 1 min. The layer of PMMA supports the good adhesion of the next layer of SU-8 and step of lift-off. Lastly, a mixture of SU-8 2000.5 and 2002 (1:1 = v:v) was spin coated at 3000 rpm for 40 s. Nanoimprint lithography (NIL) was then performed on the top SU-8 layer of films at 20 bar at 60 °C for 3 min using a lab-made mold possessing a hexagonal array of cylindrical cavities with a 1.5 μm periodicity. The flash layer of SU-8 and the layer of PMMA were removed by O_2 plasma using deep RIE (DRIE: Alcatel AMS 100 Deep Reactive Ion Etcher) followed by sputtering (Kurt Lesker PVD 75) of a Cr layer and then lift-off was performed in an acetone bath for 10 min. DRIE (O_2 gas, 1000 W coil/25 W platen) was then used to remove the bottom layer of SU-8 exposed through the Cr mask. The holes were filled with ITO (Kurt J Lesker, 99.999 % purity, 10 % SnO_2 by weight) by PLD (PVD Products Nano-PLD-1000 Pulsed Laser Deposition System) using a KrF excimer laser (248 nm, 200 mJ, 80 Hz) at 200 °C and under oxygen pressure of 20 mTorr. The laser was focused with a 60° incidence angle into the chamber and rastered over the target with a pulse influence of 0.33 J/cm^2. The substrate was positioned 8.3 cm above the target. The PLD chamber was evacuated to a base pressure of less than 6×10^{-6} Torr prior to deposition. Both the target and FTO substrate were continuously rotated at 40 and 20 rpm, respectively, during deposition. After deposition, the film was annealed at 300 °C for 30 min, followed by Cr etching and then SU-8 etching by O_2 plasma to obtain patterned ITO spikes on the FTO substrate (hereafter denoted as P-ITO substrate). Scanning electron microscopy (SEM: Hitachi S-4700 Cold Cathode Field Emission Scanning Electron Microscope, 2 kV) was employed to observe the P-ITO substrate. Absorbance of samples was measured through UV-vis spectroscopy with WinSpec32 incorporating a Labsphere RTC-060-SF to eliminate absorbance error due to reflection and scattering.

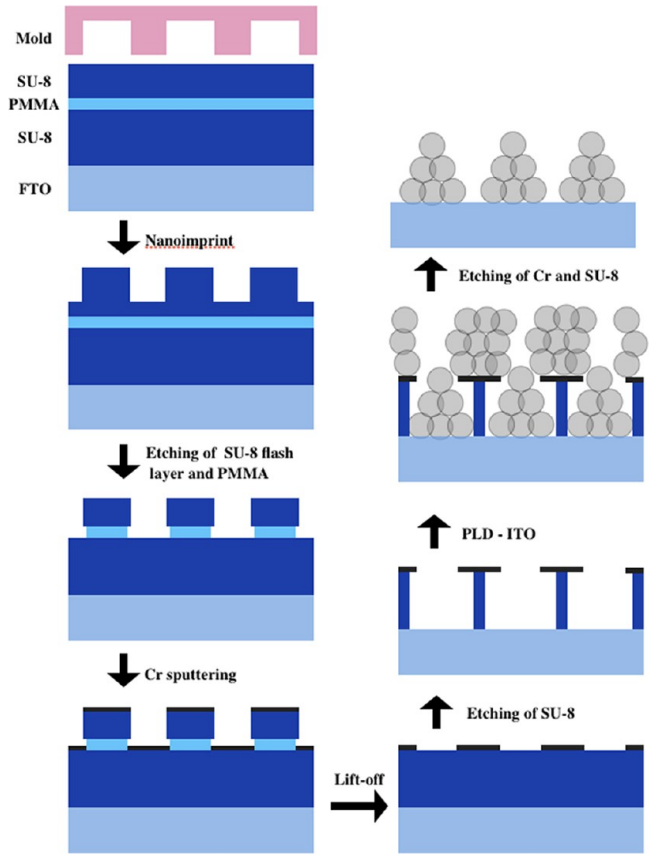

Figure 1. Schematic image of fabrication process of patterned ITO on FTO substrate.

Fabrication and Characterization of DSSCs. Tantalum doped TiO_2 (hereafter denoted as Ta:TiO_2) was deposited on FTO (control samples) and P-ITO substrates by PLD from a Ta:TiO_2 target (Kurt J Lesker, 99.999 % purity, 1 atomic % Ta) with the same laser set at 300 mJ producing a pulse influence of 0.5 J/cm^2 at 25 °C and under oxygen pressure of 100 mTorr. The substrate was positioned 5 cm above the target. The deposited films were annealed at 500 °C for 1 h by heat gun. The films were then sensitized with 0.3 mM N719 dye (Sigma-Aldrich: ditetrabutylammonium *cis*-bis(isothiocyanato)bis-(2,2′-bipyridyl-4,4′-dicarboxylato)-ruthenium(II)) in a mixed solvent of acetonitrile and *tert*-butanol (1:1 = v:v) for 20−24 h. A sandwich type cell was fabricated with Surlyn film (Solaronix, 25 μm) as a spacer between the photoanode coated with the dye sensitized Ta:TiO_2 film and platinum coated FTO counter electrode. A pre-drilled hole in the counter electrode allowed for the injection of the redox electrolyte which contained 0.03 M I_2 (Sigma-Aldrich), 0.05 M LiI (Sigma-Aldrich), 1.0 M 1,3-dimethylimidazolium iodide (Solaronix), 0.1 M guanidinium thiocyanate (Sigma-Aldrich), and 0.5 M *tert*-butylpyridine (Sigma-Aldrich) in a mixed solvent of dried acetonitrile and valeronitrile (85:15 = v:v). The electrolyte was injected by vacuum backfilling, and the hole was covered by Surlyn film and a cover glass.

Linear sweep voltammetry (LSV, current-voltage characteristic), electrochemical impedance spectroscopy (EIS), and open circuit voltage decay (OCVD) measurements were employed to characterize the device performance using a Gamry 500 potentiostat with Gamry Framework. An AM1.5 (1 sun) solar simulator (Newport 1000W Xe lamp and an AM1.5 filter) was used as the light source for device irradiation. Incident photon to current (conversion) efficiency (IPCE) measurement was also employed by using a LabVIEW controlled Keithley 2400 current meter and a 75 W Xe lamp (Oriel 6251)/monochromator (Oriel Cornerstone 260). Incident light intensity was measured using a calibrated Si-photodiode.

RESULTS AND DISCUSSION

A SEM image of the SU-8 template with the hexagonal pattern of circular holes on top of the FTO substrate is shown in Figure 2a. This hexagonal hole pattern had a pitch of 1.5 μm and was

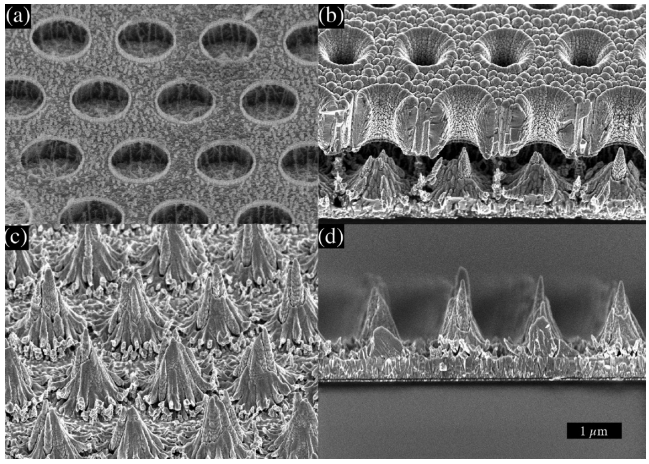

Figure 2. SEM images of template of patterned hole (a), P-ITO on FTO substrate before removal of the template (b), P-ITO on FTO substrate 45-degree view (c), and cross-sectional view (d).

600-700 nm in depth. ITO was deposited into the holes using PLD producing the ITO spikes shown in Figure 2b–d. A possible mechanism leading to the spike shape may be that the probability of ablated particles reaching the hole center is higher than that of particles which impinge onto the surrounding hole edge. The direction of the ablated particles is not fully normal to the substrate resulting in ablated particles impinging at the surface of FTO from different angles. Particles with trajectories at smaller angles to the surface are blocked by the Cr/SU-8 layer while those with more perpendicular trajectories land inside the hole on the FTO surface. Moreover, the diameter of holes became smaller because of the ITO on the top of Cr/SU-8 layer. Hence, progressively more ITO is deposited at the whole centers producing the spike-like appearance. The ITO on the Cr/SU-8 layer was removed with the chromium layer when the sample was submerged in the chromium etchant.

The resulting ITO spikes were roughly 1.5 μm in height with a pitch matching the template's of 1.5 μm. This height can of course be varied by adjusting the number of laser shots, which to achieve this height required 100,000 shots. Also it should be noted that any materials could be deposited on the SU-8 template. The sheet resistance of P-ITO substrate was slightly higher than that of the plain FTO substrate, 15.6 Ω/square compared with 11.1 Ω/square (Table 1), which may be attributed to the additional interface between FTO and ITO. Light absorbance measurements, Figure 3, show that P-ITO

Table 1. Device Performance with FTO and P-ITO Substrates

substrate	FTO	P-ITO
sheet resistance (Ω/square)	11.1	15.6
V_{oc} (V)	0.62	0.60
J_{sc} (mA/cm^2)	8.4	10.3
FF	0.62	0.51
efficiency (%)	3.2	3.2
maximum IPCE at 530 nm (%)	35.6	43.6

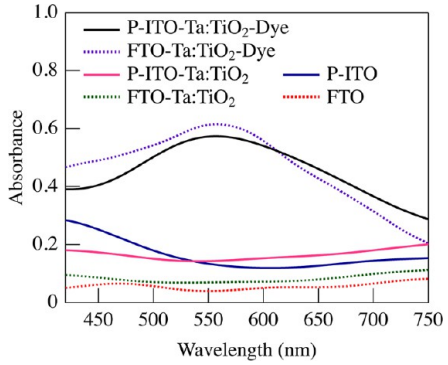

Figure 3. Absorbance of FTO (dotted red line) and P-ITO (solid blue line) substrates, and FTO-Ta:TiO_2 (dotted green line), P-ITO-Ta:TiO_2 (solid pink line), FTO-Ta:TiO_2–Dye (dotted purple line), and P-ITO-Ta:TiO_2–Dye (solid black line).

substrate (solid blue line) absorbed more light than the FTO substrate (dotted red line) at the range of wavelength measured which may be due to both the ITO spikes absorbing light themselves and also scattering the light allowing more photon absorption.

Films of Ta:TiO_2 were deposited via PLD on both FTO and the P-ITO substrates using 400,000 shots. The porosity (density) of the Ta:TiO_2 films is determined by the O_2 partial pressure in the chamber that changes the length of the ablation plume (l_p) relative to the deposition distance between target and substrate (d_{ts}).[21,22] When the target material is ablated under low pressure, the atoms/ions tend to travel in a straight path to the substrate and impinge upon it with high kinetic energies that indicates the l_p is larger than d_{ts} and allow the atoms/ions to create a dense film structure. When it is deposited under higher pressure of an added O_2 gas the ions do not travel in straight lines. The atoms/ions collide against the background gas and their kinetic energies become low (l_p is comparable to d_{ts}). Under this condition, the nucleation of seed and formation of nanocrystals occur in the plume itself. The particles have enough remaining kinetic energy to fuse and stack on one another (shadowing effect), which results in the tree-like structures.[21,23]

Higher O_2 pressure leads to a more porous (less dense) film allowing for a greater amount of dye adsorption because of the increased film surface area. However, if the film is too porous it becomes brittle, and electron transport is less efficient. In a prior study it was determined that a partial pressure of 100 mTorr produces the highest performing Ta:TiO_2 films for DSSC application possessing a morphology balancing the two aspects mentioned.[19] Figure 4 shows SEM images of Ta:TiO_2 films deposited on the plain FTO and P-ITO substrates. As can be seen, the morphology and growth pattern of Ta:TiO_2 deposited on P-ITO is markedly different from that

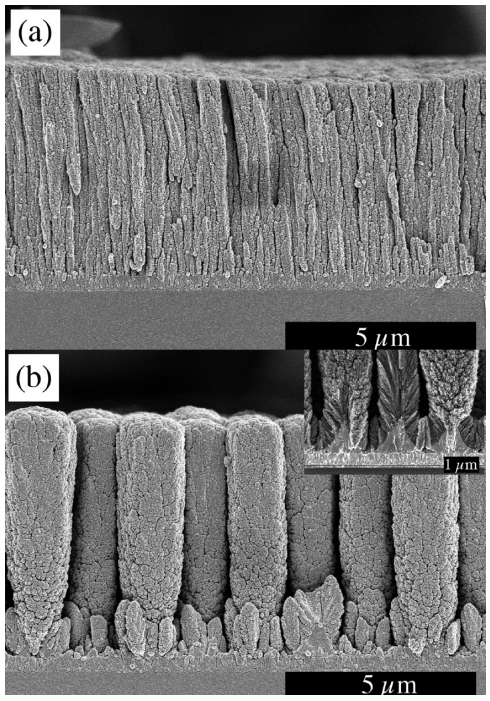

Figure 4. SEM images of Ta:TiO_2 film on (a) FTO and (b) P-ITO substrates. Inset of (b) is a SEM image of Ta:TiO_2 clearly deposited on ITO spikes.

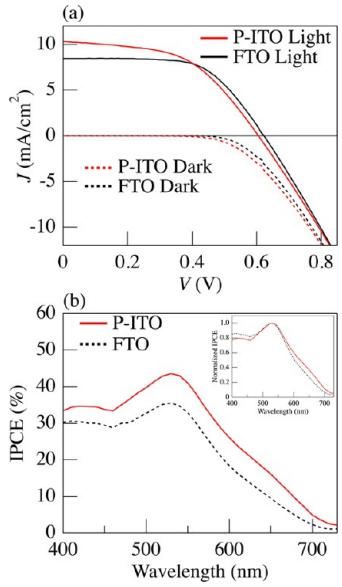

Figure 5. (a) *J-V* curves and (b) IPCE of the device with FTO (dotted black line) and P-ITO (solid red line) substrates. Inset of (b) is the normalized IPCE.

demonstrated by its deposition on plain FTO. The Ta:TiO_2 growth on the P-ITO substrate formed separated brushes with each originating from a sole ITO spike. The inset of Figure 4b clearly shows that the Ta:TiO_2 was deposited on the top of ITO spikes.

A possible mechanism leading to the separated brush-like growth may be that the spikes intercept the ablated particles impinging at an angle before they can hit the flat surface between the spikes and therefore Ta:TiO_2 particles accumulate primarily on the ITO spikes. Additionally, as growth of the Ta:TiO_2 occurs the particles are completely intercepted by the growing brushes since the particles are randomly colliding with each other and only a small percentage have a long enough free path to travel vertically to the flat surface so that the higher the trees grow the less the probability of particles reaching the surface given a fixed mean free path distribution of the particles. As for the Ta:TiO_2 films deposited on plain FTO substrate they exhibit the forest-like vertically aligned growth of nanocrystals reported previously.[19] It should be noted that although the same number of laser shots were used to deposit Ta:TiO_2 onto both plain FTO and P-ITO substrates, the height of the Ta:TiO_2 film on P-ITO tended to be thicker than the one on plain FTO. The difference in growth rate is a result of the separated brush-like structure with the Ta:TiO_2 particles preferentially landing on top of the growing brushes, but the total Ta:TiO_2 mass is the same.

After deposition of Ta:TiO_2 films on the plain FTO and P-ITO substrates they were assembled as the photoanodes into DSSCs, and photoelectrochemical tests were performed on the devices. Figure 5a presents the *J-V* performance for devices constructed on the FTO and P-ITO substrates. In particular, the J_{sc} of the device with P-ITO substrate was significantly higher than the one with FTO substrate although the values of V_{oc} were comparable, which is understandable since V_{oc} represent the potential difference between the Fermi level of electrode material and the redox potential of electrolyte, and the electrode material is the same for these two devices. Table 1 provides a summary of the device performance.

The IPCE measurements (Figure 5b) were in good agreement with the higher J_{sc} exhibited by the P-ITO device as the IPCE of the P-ITO device was larger than the plain FTO device over the entire wavelength range. To observe the major difference of IPCE as a function of wavelength, the IPCE value was normalized by the maximum IPCE, at 530 nm. This normalized IPCE (inset of Figure 5b) showed that a higher IPCE enhancement was obtained in the 550−730 nm range for the P-ITO than the plain FTO device. Greater light absorption in the dye loaded film on P-ITO in approximately the same wavelength range, 600−750 nm, was indicated in the absorption spectra shown in Figure 3. The enhanced absorption may be attributed to the increased light scattering and trapping by the patterned ITO spikes. Another benefit of P-ITO spikes structure which may also contribute to the higher J_{sc} may arise from the restricted lateral dimensions of the individual brushes. Electrons injected into the Ta:TiO_2 film exhibit random-walk behavior until they reach the conductive oxide electrode (or any collector) so that electrons move not only vertically but also laterally. This means that injected electrons which are allowed to freely move laterally for a given electron path length may be less likely to reach the electrode than electrons whose lateral movements are restricted and effectively "funneled" to the electrode. Previous groups have attempted to employ this concept by fabricating 1-dimensional nanowire arrays grown vertically from transparent conducting electrodes.[13] However, efficiencies from DSSC devices assembled from these films were low because of the low surface area available for dye loading. In the present study the separated brush structure should restrict the lateral movement of electrons especially given the relatively large spacing between the Ta:TiO_2 brushes and their small diameters. Therefore, the larger J_{SC} may be due to a greater efficiency in electron capture. SEM was used to investigate the possibility of any morphological changes to the electrode after the photo-

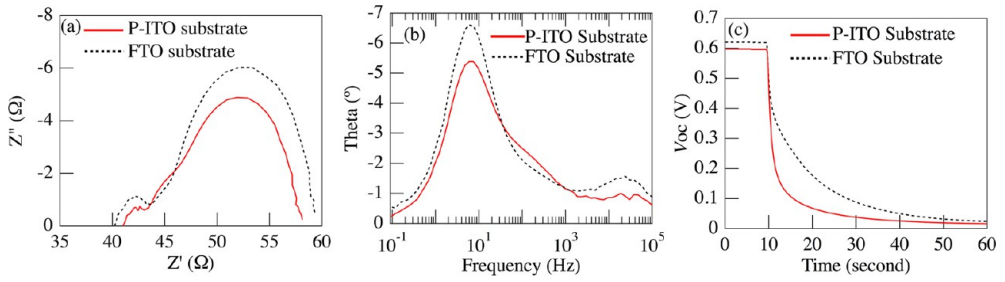

Figure 6. (a) Nyquist and (b) Bode plots from EIS, and (c) OCVD response for DSSCs with FTO (dotted black line) and P-ITO (solid red line) substrates.

electrochemical measurements were performed and no noticeable mechanical degradation of the electrode was observed (data not shown).

However, the fill factor (FF) was lower for the device assembled from the P-ITO substrate than the one assembled from the plain FTO substrate. Causes of low FF are typically high resistance of electrode/dye/electrolyte interface and/or loss of excited electrons (e.g. via recombination) in a device. EIS and OCVD measurements were employed to further investigate the potential source of the lower FF value for the P-ITO device (Figure 6). The Nyquist plot (Figure 6a) indicates a lower resistance of the electrode/dye/electrolyte interface for the P-ITO substrate device than for the plain FTO substrate device suggesting that this is not the cause for the smaller fill factor of P-ITO device. Furthermore, the peak maxima frequencies of these devices from a Bode plot were both 6 s^{-1} (Figure 6b). This frequency is equal to the rate constant for the recombination of injected electrons in a semiconducting film with tri-iodide in the electrolyte which is inversely proportional to electron lifetime in the film.[24,25] Therefore the electron recombination rate in the Ta:TiO_2 films was similar for the patterned and un-patterned films. OCVD measurements (Figure 6c) show a faster voltage decay for the device with P-ITO substrate than the one with FTO substrate; this corresponds to a higher rate of loss of electrons in the P-ITO device. Since the recombination rate at the interface of electrode/dye/electrolyte for both devices was the same, the faster rate of recombination for the former device could be attributed to the back-electron transfer at the FTO surface. In the literature, Intensity-Modulated Infrared Spectroscopy analysis for DSSC showed that recombination occurs predominantly in the region of the FTO surface rather than across the depth of the TiO_2 film.[26] To avoid this issue, a blocking layer is deposited prior to an electrode deposition.[27] In this work, there was no blocking layer. As seen in the SEM image (Figure 4b), the structure of Ta:TiO_2 film on P-ITO substrate was more open and the little amount of Ta:TiO_2 deposited between the brushes appears to be non-continuous and highly porous. The electrolyte can easily migrate into the film and make direct contact with the FTO surface. Hence a greater amount of back-electron transfer at the FTO/electrolyte interface likely occurred in the device with P-ITO substrate resulting in the lower FF. It should be noted that the open structure could be useful for DSSCs with solid electrolytes. It is difficult to introduce a solid electrolyte to DSSC's system since films mostly used are dense and the solid electrolyte cannot be filled inside of the film. This open structure may be promising for this application.

In addition to the back-electron transfer at the FTO surface, it is possible that the interface between the ITO and FTO may have contributed to the low FF of the P-ITO device because of increased resistive losses. The ITO/FTO interfaces may manifest as an additional semicircle and peak appearing in the hundredth region of the Nyquist and Bode plot, respectively, of the P-ITO device, which was not observed in the EIS spectra of the plain FTO device. Although the device with P-ITO substrate did not demonstrate a higher overall conversion efficiency because of its lower FF, a higher J_{sc} was obtained from the device and further improvement may be possible by introduction of a blocking layer on top of the P-ITO substrate prior to Ta:TiO_2 deposition by PLD.

CONCLUSIONS

In conclusion, we successfully fabricated a patterned ITO substrate via nanoimprint lithography and pulsed laser deposition. The patterned ITO consisted of 1.5 μm tall spikes arranged hexagonally on an FTO substrate. The height of ITO spikes was controlled by varying the number of PLD shots. Additional deposition of Ta:TiO_2 via PLD on top of these patterned substrates resulted in the growth of separate brush-like structures originating from the tips of the ITO spikes. A conversion efficiency of 3.2% was obtained from DSSCs fabricated using these patterned substrates equal to the conversion efficiency of DSSCs fabricated from plain FTO substrates. The J_{SC} of the patterned DSSCs was 25% larger than the un-patterned device; however, the patterned device exhibited a lower FF offsetting the increase in J_{SC} leading to the equality in efficiencies. Further optimization of the patterned substrate, including the introduction of a blocking layer, may lead to improvement in the FF. We believe that the patterned ITO substrate can be used for other forms of solar cells and applications. Specifically, the open brush-like structure of the Ta:TiO_2 film may allow for better infiltration of various ionic polymers or small molecule hole conductors utilized in solid-state DSSCs.

AUTHOR INFORMATION

Corresponding Author

*E-mail: hara@live.unc.edu.

Present Address

[§]Department of Mechanical Engineering, Cockrell School of Engineering, University of Texas at Austin, Austin, Texas, U.S.A.

Author Contributions

The manuscript was written through contributions of all authors. All authors have given approval to the final version of the manuscript.

Notes

The authors declare no competing financial interest.

■ ACKNOWLEDGMENTS

This material is based upon work funded by the U.S. Department of Energy, Office of Science, Office of Basic Energy Sciences, under Award Number DE-SC0006416. We also acknowledge support for the use of instrumentation and help with device assembly and evaluation to the UNC EFRC (Center for Solar Fuels, an Energy Frontier Research Center funded by the U.S. Department of Energy, Office of Science, Office of Basic Energy Sciences, under Award Number DE-SC0001011) and from UNC SERC ("Solar Energy Research Center Instrumentation Facility" funded by the U.S. Department of Energy, Office of Energy Efficiency & Renewable Energy under Award Number DE-EE0003188). L.A. wishes to acknowledge financial support from research triangle solar fuels institute (RTSFI). The authors would also like to thank Chapel Hill Analytical and Nanofabrication Laboratory (CHANL) for all their assistance.

■ REFERENCES

(1) Oregan, B.; Grätzel, M. *Nature* **1991**, *353*, 737−740.
(2) Wei, D. *Int. J. Mol. Sci.* **2010**, *11*, 1103−1113.
(3) Kong, F.-T.; Dai, S.-Y.; Wang, K.-J. *Adv. Optoelectron.* **2007**, *2007*, 1−14.
(4) Grätzel, M. *J. Photochem. Photobiol., C* **2003**, *4*, 145−153.
(5) Nakade, S.; Saito, Y.; Kubo, W. *J. Phys. Chem. B* **2004**, *108*, 1628−1633.
(6) Oregan, B.; Moser, J.; Anderson, M. *J. Phys. Chem.* **1990**, *94*, 8720−8726.
(7) Sodergren, S.; Haffeldt, A.; Olsson, J. *J. Phys. Chem.* **1994**, *98*, 5552−5556.
(8) Nakade, S.; Saito, Y.; Kubo, W.; Kitamura, T.; Wada, Y.; Yanagida, S. *J. Phys. Chem. B* **2003**, *107*, 8607−8611.
(9) Leng, W. H.; Barnes, P. R. F.; Juozapavicius, M.; O'Regan, B. C.; Durrant, J. R. *J. Phys. Chem. Lett.* **2010**, *1*, 967−972.
(10) Yin, Y.; Tan, X.; Hou, F.; Zhao, L. *Front. Chem. Eng. China* **2009**, *3*, 298−304.
(11) Yang, W.; Wan, F.; Wang, Y.; Jiang, C. *Appl. Phys. Lett.* **2009**, *95*, 133121_1−133121_3.
(12) Jin, L.; Zhai, J.; Heng, L.; Wei, T.; Wen, L.; Jiang, L.; Zhao, X.; Zhang, X. *J. Photochem. Photobiol., C* **2009**, *10*, 149−158.
(13) Law, M.; Greene, L. E.; Johnson, J. C.; Saykally, R.; Yang, P. *Nat. Mater.* **2005**, *4*, 455−9.
(14) Bouclé, J.; Snaith, H. J.; Greenham, N. C. *J. Phys. Chem. C* **2010**, *114*, 3664−3674.
(15) Zhang, Q.; Dandeneau, C. S.; Zhou, X.; Cao, G. *Adv. Mater.* **2009**, *21*, 4087−4108.
(16) Sauvage, F.; Di Fonzo, F.; Bassi, A. L.; Casari, C. S.; Russo, V.; Divitini, G.; Ducati, C.; Bottani, C. E.; Comte, P.; Graetzel, M. *Nano Lett.* **2010**, *10*, 2562−2567.
(17) Noh, J. H.; Park, J. H.; Han, H. S.; Kim, D. H.; Han, B. S.; Lee, S.; Kim, J. Y.; Jung, H. S.; Hong, K. S. *J. Phys. Chem. C* **2012**, *116*, 8102−8110.
(18) Ghosh, R.; Brennaman, M. K.; Uher, T.; Ok, M.-R.; Samulski, E. T.; McNeil, L. E.; Meyer, T. J.; Lopez, R. *ACS Appl. Mater. Interfaces* **2011**, *3*, 3929−35.
(19) Ghosh, R.; Hara, Y.; Alibabaei, L.; Hanson, K.; Rangan, S.; Bartynski, R.; Meyer, T. J.; Lopez, R. *ACS Appl. Mater. Interfaces* **2012**, *4*, 4566−70.
(20) Wang, F.; Subbaiyan, N. K.; Wang, Q.; Rochford, C.; Xu, G.; Lu, R.; Elliot, A.; D'Souza, F.; Hui, R.; Wu, J. *ACS Appl. Mater. Interfaces* **2012**, *4*, 1565−72.
(21) Ghosh, R.; Brennaman, M. K.; Concepcion, J. J.; Hanson, K.; Kumbhar, A. S.; Meyer, T. J.; Lopez, R. *Proc. SPIE* **2011**, *8109*, 81090U-1−81090U-6.
(22) Bailini, A.; Di Fonzo, F.; Fusi, M.; Casari, C. S.; Bassi, A. L.; Russo, V.; Baserga, A.; Bottani, C. E. *Appl. Surf. Sci.* **2007**, *253*, 8130−8135.
(23) Vo Thi, T. H.; Rouet, J.-L.; Brault, P.; Bauchire, J.-M.; Cordier, S.; Josserand, C. *J. Phys. D: Appl. Phys.* **2008**, *41*, 022003.
(24) Adachi, M.; Sakamoto, M.; Jiu, J.; Ogata, Y.; Isoda, S. *J. Phys. Chem. B* **2006**, *110*, 13872−80.
(25) Hoshikawa, T.; Yamada, M.; Kikuchi, R.; Eguchi, K. *J. Electrochem. Soc.* **2005**, *152*, E68.
(26) Zhu, K.; Schiff, E. a.; Park, N.-G.; van de Lagemaat, J.; Frank, A. J. *Appl. Phys. Lett.* **2002**, *80*, 685.
(27) Ito, S.; Murakami, T. N.; Comte, P.; Liska, P.; Grätzel, C.; Nazeeruddin, M. K.; Grätzel, M. *Thin Solid Films* **2008**, *516*, 4613−4619.